Pergamon

Acta mater. 49 (2001) 1479–1493

Acta MATERIALIA

www.elsevier.com/locate/actamat

DISLOCATION BOUNDARIES—THE DISTRIBUTION FUNCTION OF DISORIENTATION ANGLES

W. PANTLEON† and N. HANSEN

Materials Research Department, Risø National Laboratory, P.O. Box 49, DK-4000 Roskilde, Denmark

(Received 28 June 2000; received in revised form 28 December 2000; accepted 28 December 2000)

Abstract—In dislocation structures orientation differences arise across dislocation boundaries during plastic deformation. The distribution function of the disorientation angles related to dislocation boundaries has been determined empirically and is almost independent of experimental parameters such as material type, plastic strain, temperature and deformation conditions (Hughes et al., Phys. Rev. 81 (1998) 4664). In the present paper distribution functions are derived from geometrical considerations for quite general assumptions on the number of sets of parallel dislocations and their arrangement. The relation between the obtained distribution functions for the disorientation angles and general orientation distributions is elucidated. A comparison with the experimental results shows that the Rayleigh distribution obtained for an equivalent contribution from two dislocation sets with perpendicular rotation axes is most appropriate for describing the experimental data. For experimental distributions with a larger spread in the disorientation angles and relatively large deviations from a Rayleigh distribution a superposition of two Rayleigh distributions is suggested implying the presence of two different types of boundaries in a given structure. Finally, it is shown that an analysis of distribution functions of disorientation angles can further the understanding of deformation induced structural changes.

Zusammenfassung—Während plastischer Verformung treten in Versetzungsstrukturen Orientierungsunterschiede auf. Die Verteilung der Fehlorientierungswinkel von Versetzungsgrenzen wurde empirisch ermittelt und erweist sich als nahezu unabhängig von den experimentellen Parametern wie Werkstoff, Dehnung, Temperatur oder den konkreten Verformungsbedingungen (Hughes et al., Phys. Rev. 81 (1998) 4664). In dieser Arbeit werden Verteilungsfunktionen der Desorientierungswinkel aus geometrischen Überlegungen für allgemein gehaltene Annahmen über die Zahl der enthaltenen Sätze paralleler Versetzungen und deren Anordnung abgeleitet. Der Zusammenhang zwischen den abgeleiteten Verteilungsfunktionen der Desorientierungswinkel und allgemeinen Orientierungsverteilungsfunktionen wird dargelegt. Ein Vergleich mit experimentellen Ergebnissen zeigt, daß Rayleigh-Verteilungen, die von gleichberechtigten Beiträgen zweier Sätze von Versetzungen mit orthogonaler Drehachse rühren, zur Beschreibung der experimentellen Daten am besten geeignet sind. Für experimentell gefundene Verteilungen, die eine breitere Streuung zeigen und auch größere Abweichungen von einer Rayleigh-Verteilung aufweisen, wird die Überlagerung zweier Rayleigh-Verteilungen vorgeschlagen und damit die Annahme zweier unterschiedlicher Arten von Versetzungsgrenzen in der Versetzungsstruktur impliziert. Schließlich wird gezeigt, daß eine Analyse der Verteilungsfuntionen der Desorientierungswinkel förderlich für die Erklärung verformungsinduzierter Änderungen in der Substruktur ist.

Keywords: Dislocations; Microstructure; Disorientations; Mechanical properties, plastic; Theory & modelling

1. INTRODUCTION

Deformation-induced dislocation boundaries are characteristic for plastically deformed metals and alloys. Such boundaries have different features and two different types of boundaries can be distinguished [1]: ordinary cell boundaries (incidental dislocation boundaries, IDBs) arising from a statistical mutual trapping of dislocations and geometrically necessary boundaries (GNBs) caused by different activities on the slip systems on either side of the boundary. Orientation differences between regions separated by dislocation boundaries arise and disorientations are connected with boundaries of both types: disorientation angles across IDBs are relatively small with a narrow spread, whereas the disorientation angles across GNBs can have a much wider spread and their average disorientation angle is larger than that of IDBs.

For the distribution functions $f(\theta)$ (i.e. the continuous probability density function or, alternatively, the discrete probability densities p) of the disorientation angles θ across both types of boundaries scaling was established based on experimental data on cold-rolled

† To whom all correspondence should be addressed.

E-mail address: wolfgang.pantleon@risoe.dk (W. Pantleon)

1359-6454/01/$20.00
PII: S1359-6454(01)00027-1

pure aluminium polycrystals [2]: The distribution functions determined after different plastic strains (rolling reductions) coincide after a normalization of the disorientation angles by their respective average angle $\bar{\theta}$ according to

$$\hat{f}(x) = f(\theta)\frac{\mathrm{d}\theta}{\mathrm{d}x} = \bar{\theta}f(x\bar{\theta}) \quad \text{with } x = \theta/\bar{\theta}. \tag{1}$$

This is valid on the condition that IDBs and GNBs are treated separately as scaling does not occur, if all boundaries are grouped together. Figure 1 illustrates this behaviour for IBDs and GNBs in aluminium cold-rolled to different strains.

The same behaviour was found for IDBs in copper single crystals [3, 4] (after hot-compression) and was also confirmed for nickel (rolling) and a stainless steel (compression) [5]. Although observed in different materials all distributions for IDBs (ordinary cell boundaries [1]) normalized by their average angle fall on the same master curve [5].

In previous papers [3, 4] the shape of the distribution and the scaling (for small disorientation angles) were traced to a simple geometrical reason: the existence of two inclined dislocation sets in each boundary. The purpose of the present paper is to extend the previous analysis to more than two dislocation sets and to address some apparent limitations of the approach. The basic idea is to explore the general possibilities rather than a consideration of specific dislocation arrangements resulting from certain activated slip systems. In this manner, the investigation is not restricted to any particular deformation mode.

First, the analysis is limited to small disorientation angles, before the occurrence of higher disorientation angles is taken into account. This allows the theoretical distributions to be compared with experimental observations showing a relatively large variation in disorientation angles and angular spread. The comparison shows that distribution functions can be a useful tool in the analysis of formation and evolution of dislocation boundaries.

2. SMALL DISORIENTATION ANGLES

2.1. A single dislocation set

Disorientations across IDBs arise from statistical fluctuations in the dislocation fluxes passing the boundaries. For a single activated slip system only a single set of dislocations is stored in the boundary and a Gaussian distribution $f_{G,\sigma_\alpha}(\alpha)$ for the disorientation angles α results with vanishing mean value and a standard deviation σ_α depending on plastic strain [6]. In case of GNBs disorientations are caused by an imbalance between activities of the slip system on both sides of the boundaries. In a deformation structure the imbalances are not the same across each GNB, for instance, both positive and negative imbalances are required in order to avoid an overall bend-

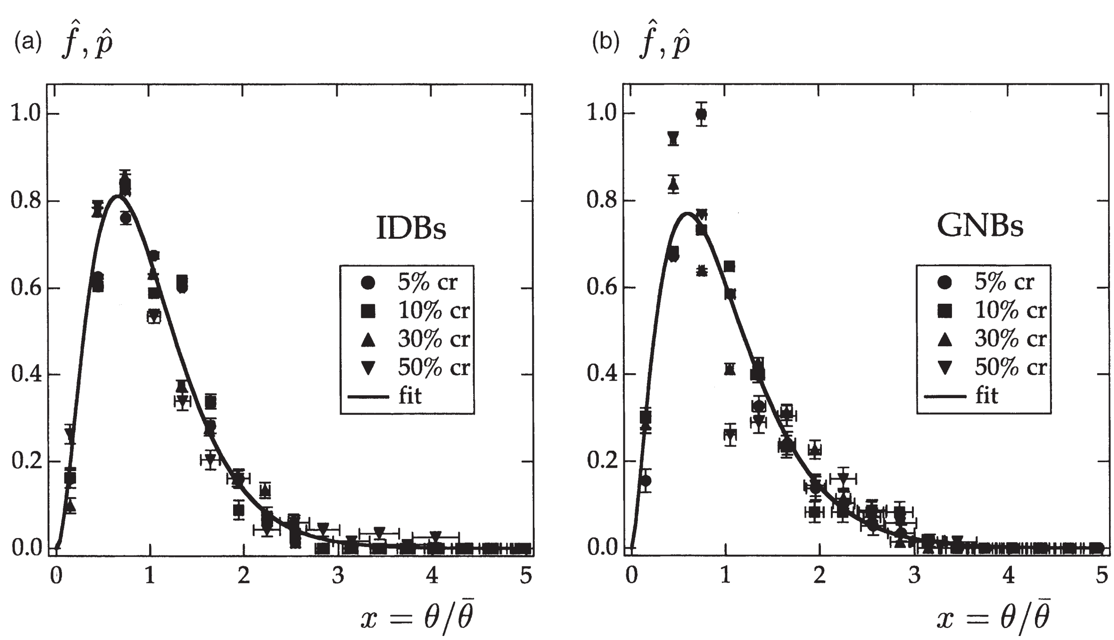

Fig. 1. Histograms (relative frequencies $\hat{p}_i = \bar{\theta}p_i$ of finding a normalized disorientation angle $x = \theta/\bar{\theta}$ within a bin of width $\Delta x \approx 1/3$) of the disorientation angles normalized by the average disorientation angle $\bar{\theta}$ for different types of boundaries in cold-rolled aluminium after different rolling reductions: (a) incidental dislocation boundaries; and (b) geometrically necessary boundaries (from Ref. [2]). The solid lines represent an empirical fit of a distribution $\hat{f}(x) = a^a x^{a-1}\exp(-ax)/\Gamma(a)$ with $a = 3$ for IDBs and $a = 2.5$ for GNBs (this distribution will not be discussed further; it was suggested [2] by an analogy to the analysis of island growth, without direct correspondence to the dislocations accumulated in a boundary).

ing. A statistical distribution of different imbalances across different GNBs in the deformation structure leads to a Gaussian distribution of the disorientation angle with vanishing mean value for GNBs also [7], but with a stronger increase of the standard deviation with plastic strain than for IDBs [7, 8].

A single dislocation set in the boundaries is expected only for a single activated slip system and therefore restricted to single glide in single crystals. In unidirectional deformation, no boundary formation is found in single glide. The predicted Gaussian distribution of the disorientation angle may be observable only in cyclic deformation where a single activated slip system leads to the formation of dislocation walls. On the other hand, in cyclic deformation the evolution of the disorientation angle is strongly retarded [8].

In polycrystals and even in single crystals after the onset of secondary glide plastic deformation is carried by several slip systems and several sets of dislocations are accumulated in the boundaries. The consequences of having more than a single dislocation set in the boundaries are investigated. In the following, it is assumed that the contribution of each dislocation set to the disorientation of the boundary is statistically equivalent, a generalization to non-equivalent contributions is outlined in Appendix A.

2.2. *Two inclined dislocation sets*

For a theoretical description of the shape of the distribution function two sets of inclined edge dislocations in the boundaries have been considered [3, 4] as shown in Fig. 2. This idea, which also explains the scaling behaviour, is summarized shortly.

Each set i of parallel edge dislocations of Burgers vector $\vec{b}_i$ (perpendicular to the boundary plane) with a mutual distance h_i in a boundary contributes to the total disorientation across the boundary with a rotation around a rotation axis $\vec{u}_i$ by an angle $\alpha_i = b_i/h_i$ [9]. If a dislocation boundary consists of two dislocation sets only, the common disorientation angle θ is defined by the individual disorientation angles α_1 und α_2 and an inclination angle β between the two rotation axes ($\cos\beta = \vec{u}_1 \cdot \vec{u}_2$):

$$\cos(\theta/2) = \cos(\alpha_1/2)\cos(\alpha_2/2) - \sin(\alpha_1/2)\sin(\alpha_2/2)\cos(\beta). \quad (2)$$

For small disorientation angles θ and α_i the trigonometric functions are replaced by the first terms of a Taylor expansion:

$$\theta^2 = \alpha_1^2 + \alpha_2^2 + 2\alpha_1\alpha_2\cos(\beta). \quad (3)$$

It is assumed that both dislocation sets contribute in an equal manner and the disorientation angles α_i of each individual dislocation set are Gaussian distributed (e.g. for IDBs from statistical fluctuations in the dislocation fluxes passing through the dislocation boundaries [6, 7]) with vanishing mean values and the same standard deviation σ_α. From the probability of finding a disorientation angle less than θ

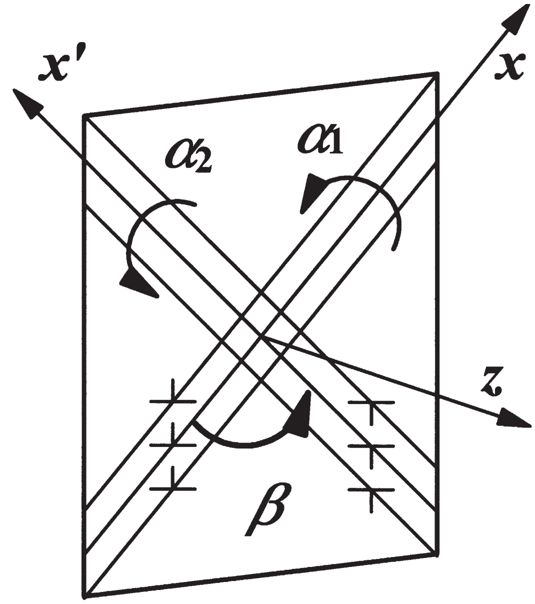

Fig. 2. Schematic view of a tilt boundary composed by two sets of parallel edge dislocations. Both dislocation sets have the same Burgers vector $\vec{b}$ (parallel to the boundary normal z). Each set causes a rotation around an axis parallel to the dislocation line (x or x' axis). The dislocation lines are inclined towards each other by an angle β. The line direction of one set (x) is pointing towards the drawing plane, the other (x') outwards causing the apparent opposite sign of the dislocations (from Ref. [3]).

$$\mathrm{P}(X<\theta) = \int\int_{\theta^2>\alpha_1^2+\alpha_2^2+2\alpha_1\alpha_2\cos(\beta)} f_{\mathrm{G},\sigma_\alpha}(\alpha_1) f_{\mathrm{G},\sigma_\alpha}(\alpha_2)\,\mathrm{d}\alpha_1\,\mathrm{d}\alpha_2 \quad (4)$$

the distribution function†

$$f_\beta(\theta) = \frac{\mathrm{dP}}{\mathrm{d}\theta} = \frac{\theta}{\sigma_\alpha^2\sin\beta}\exp\left(-\frac{\theta^2}{2\sigma_\alpha^2\sin^2\beta}\right)I_0\left(\frac{\theta^2\cos\beta}{2\sigma_\alpha^2\sin^2\beta}\right) \quad (5)$$

is obtained [3].

The distribution of equation (5) causes a proportionality of the moments of order m of the disorientation angle to the power m of the standard deviation σ_α

$$\langle\theta^m\rangle \propto \sigma_\alpha^m \propto \bar{\theta}^m \quad (6)$$

where the brackets $\langle\cdot\rangle$ denote ensemble averages.

† Note, the setting error in equation (19) in Ref. [3] for the scaled distribution $\hat{f}(x)$ where $\sin\beta^2$ has to be corrected to $(\sin\beta)^2 = \sin^2\beta$.

Consequently, normalization of the disorientation angle by the average angle $\bar{\theta} = \langle\theta\rangle$ removes all dependence on the standard deviation and the resulting distributions

$$\hat{f}_\beta(\theta/\bar{\theta}) = f_\beta(\theta)\frac{\mathrm{d}\theta}{\mathrm{d}x} = \bar{\theta}f_\beta(x\bar{\theta}) \tag{7}$$

show scaling for any inclination angle β between the rotation axes.

For the case of two perpendicular sets of edge dislocations, i.e. $\beta = 90°$ between the rotation axes, the distribution of equation (5) is simplified considerably resulting in the Rayleigh distribution

$$f_{90°}(\theta) = \frac{\theta}{\sigma_\alpha^2}\exp\left(-\frac{\theta^2}{2\sigma_\alpha^2}\right) = f_\mathrm{R}(\theta) \tag{8}$$

which is well known for grain size distributions (e.g. Ref. [10]). With $\bar{\theta} = \sigma_\alpha\sqrt{\pi/2}$ and $x = \theta/\bar{\theta}$ the scaled Rayleigh distribution becomes

$$\hat{f}_\mathrm{R}(x) = \bar{\theta}f_\mathrm{R}(x\bar{\theta}) = \frac{\pi x}{2}\exp\left(-\frac{\pi x^2}{4}\right). \tag{9}$$

2.2.1. Example. An example for deposition of two similar sets of edge dislocations in the same boundary as shown in Fig. 2 is simple shear of a face centred cubic crystal along the (001) plane in the [110] direction. Of the 12 possible slip systems of $\langle 110\rangle\{111\}$ type only two systems are activated. Both have the same Burgers vector $\vec{b} = [110]a/2$ and differ in the slip plane normal ($\vec{n}_1 = (1\bar{1}1)/\sqrt{3}$ or $\vec{n}_2 = (1\bar{1}\bar{1})/\sqrt{3}$). In boundaries on the (110) plane perpendicular to the shear direction ($\vec{n}_\mathrm{b} = (110)/\sqrt{2}$), edge dislocations of both slip systems are stored. Their line vectors are inclined towards each other with $\cos\beta = (\vec{n}_1\times\vec{n}_\mathrm{b})\cdot(\vec{n}_2\times\vec{n}_\mathrm{b})/|\vec{n}_1\times\vec{n}_\mathrm{b}|\,|\vec{n}_2\times\vec{n}_\mathrm{b}| = 1/3$ corresponding to an inclination angle β of about 70.5°.

2.2.2. Boundary character. Originally [3], the occurrence of two dislocation sets with inclined rotation axes was illustrated by a tilt boundary with two independent sets of edge dislocations. But this is not a necessary restriction and the same formulation is valid if the total disorientation between the adjacent cells is a superposition of a tilt and a twist component: The tilt component may be formed by a single set of edge dislocations leading to a rotation axis along their line vector. For the independent twist component screw dislocations in the boundary are required causing a rotation with an axis perpendicular to the boundary. For boundaries with mixed character the disorientation angle distribution is given by the Rayleigh distribution as well, because the axes of both rotations are perpendicular. It is immaterial for the considerations here, that the twist component is due to two (or more) correlated sets of parallel screw dislocations with different orientations in the boundary. With respect to their effect on the rotations they can be treated as a single independent set. Moreover, possible dislocation reactions will not alter the disorientation of the boundary.

2.3. Three perpendicular dislocation sets

Beyond that, there might be a third set of dislocations leading to a third axis of rotation. For instance, beside two edge dislocation sets leading to two inclined rotation axes in the boundary, there might be screw dislocations in the boundary leading to a third independent rotation axis perpendicular to the boundary. Even in this case, the problem can be treated for small disorientation angles by the same methods [3] as in case of two sets, but in most cases the integrals can not be solved analytically (compare Appendix A).

However, if all three rotation axes are perpendicular towards each other and each dislocation set contributes in an equal manner, i.e. the disorientation angle α_i of each individual contribution is Gaussian distributed with a vanishing mean value and the same standard deviation σ_α, the integration is straightforward and a Maxwell distribution

$$f_\mathrm{M}(\theta) = \sqrt{\frac{2}{\pi}}\frac{\theta^2}{\sigma_\alpha^3}\exp\left(-\frac{\theta^2}{2\sigma_\alpha^2}\right) \tag{10}$$

results (i.e. the same distribution as for the speed of molecules in an ideal gas). From the expectation values of order m

$$\langle\theta^m\rangle = \frac{2}{\sqrt{\pi}}2^{m/2}\sigma_\alpha^m\Gamma\left(\frac{m+3}{2}\right)\propto\sigma_\alpha^m \tag{11}$$

(with the Gamma function Γ) and their proportionality to σ_α^m or $\bar{\theta}^m$, respectively, it becomes obvious that the Maxwell distribution shows scaling, because all effects from the standard deviation can be eliminated by normalization of the disorientation angle by the average angle.

With $\bar{\theta} = \sigma_\alpha\sqrt{8/\pi}$ and $x = \theta/\bar{\theta}$ the scaled Maxwell distribution

$$\hat{f}_\mathrm{M}(x) = \bar{\theta}f_\mathrm{M}(x\bar{\theta}) = \frac{32x^2}{\pi^2}\exp\left(-\frac{4x^2}{\pi}\right) \tag{12}$$

results. As obvious from Fig. 3, this scaled distribution has some significant differences compared to the scaled Rayleigh distribution of equation (9). Especially, the maximum $\hat{f}_\mathrm{max} = \hat{f}(x_\mathrm{max})$ of the scaled Maxwell distribution is higher and shifted towards larger normalized disorientation angles x_max. Furthermore, the scaled Maxwell distribution is not as wide as the scaled Rayleigh distribution and has a smaller standard deviation (compare Table 1).

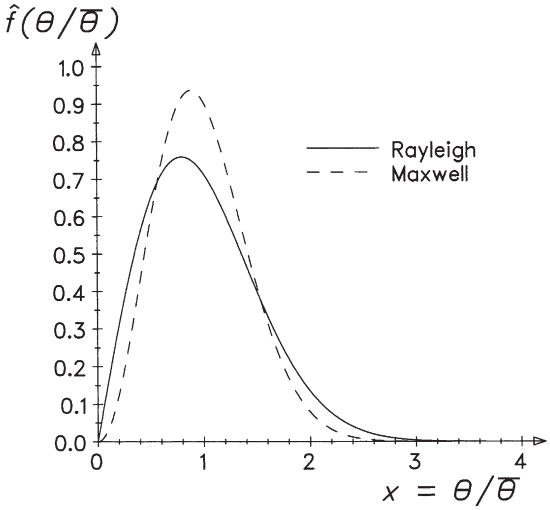

Fig. 3. Comparison of the scaled Rayleigh (equation (9)) and the scaled Maxwell distribution (equation (12)).

Table 1. Comparison of characteristic measures (position $x_{\max}$ and height $\hat{f}(x_{\max})$ of maximum, estimation value $\langle x^2\rangle$) of scaled Maxwell and Rayleigh distribution (note that the square of the standard deviation is given by $\langle(x-\langle x\rangle)^2\rangle = \langle x^2\rangle - \langle x\rangle^2 = \langle x^2\rangle - 1$)

Measure	Maxwell		Rayleigh
$x_{\max}$	$\sqrt{\pi}/2\approx 0.886$	>	$\sqrt{2/\pi}\approx 0.798$
$\hat{f}(x_{\max})$	$8/e\pi\approx 0.937$	>	$\sqrt{\pi/2e}\approx 0.760$
$\langle x^2\rangle$	$3\pi/8\approx 1.18$	<	$4/\pi\approx 1.27$

2.4. Scaling

According to equations (9) and (12) the dependence of the distribution functions $f_R(\theta)$ and $f_M(\theta)$ on the standard deviation σ_α or on the average disorientation angle $\bar{\theta}$ are eliminated by normalization of the disorientation angle by its average and the scaled distribution functions $\hat{f}(x)$ are independent of σ_α or $\bar{\theta}$. Consequently, both the Rayleigh and the Maxwell distribution show scaling behaviour.

Scaling for small disorientation angles is invoked directly by the usage of equation (3) because multiplication of each disorientation angle α_i by a common factor leads to a multiplication of the resultant disorientation angle by the same factor. This is different for larger disorientation angles, because the periodicity and the involved trigonometric functions in equation (2) prevent the distributions from true scaling at larger angles.

3. HIGH DISORIENTATION ANGLES

The distributions of disorientation angles were determined from geometrical arguments and statistical assumptions in the previous section (and Refs. [3, 4]) on the premise of small disorientations only. For larger disorientation angles† the trigonometric functions in equation (2) cannot be restricted to the leading orders of the Taylor series. An extension of the calculation to higher disorientation angles based on equation (2) could not be achieved analytically. In an alternative manner, disorientation distributions are derived in this section from the orientations of individual regions. For the distribution of these orientations a well-known orientation distribution in orientation space, the Bingham or Watson distribution, is assumed. It will be shown that the Rayleigh and the Maxwell distribution are asymptotic representations for low disorientation angles.

3.1. Description of rotations as quarternions

Orientations are determined by a rotation of an angle ω around an axis $\vec{u}$ (on the unit sphere S^3 in R^3) from a reference orientation. They can be described by unit quarternions (e.g. Ref. [11])

$$\boldsymbol{x} = \begin{pmatrix} x_0 \\ x_1 \\ x_2 \\ x_3 \end{pmatrix} = \begin{pmatrix} x_0 \\ \vec{x} \end{pmatrix} \tag{13}$$

$$= \begin{pmatrix} \cos(\omega/2) \\ \vec{u}\sin(\omega/2) \end{pmatrix} = \begin{pmatrix} \cos(\omega/2) \\ \sin(\omega/2)\sin\vartheta\cos\phi \\ \sin(\omega/2)\sin\vartheta\sin\phi \\ \sin(\omega/2)\cos\vartheta \end{pmatrix}$$

on a unit hypersphere S^4 in four dimensions. Since the quarternion $\boldsymbol{x}$ and its negative $-\boldsymbol{x}$ represent the same orientation, only the positive hemisphere S_+^4 is required with $0\le\omega<\pi$, $0\le\vartheta<\pi$ and $0\le\phi<2\pi$. The respective volume element on S_+^4 is

$$dV = \sin^2(\omega/2)\sin\vartheta\, d\omega\, d\vartheta\, d\phi. \tag{14}$$

The disorientation between two orientations $\mathbf{R}'$ and $\mathbf{R}''$ is found from the rules for performing successive rotations $\mathbf{R}''(\mathbf{R}')^{-1}$ leading to a disorientation angle θ given by

$$\cos(\theta/2) = x''_0 x'_0 + \vec{x}''\cdot\vec{x}' = \boldsymbol{x}''\cdot\boldsymbol{x}'. \tag{15}$$

3.2. Distribution function in orientation space

For the calculation of the disorientation distribution from orientations of individual regions (separated by dislocation boundaries) the common Bingham distribution [12] is considered for the distribution of their orientations. This orientation distribution can be obtained from a maximum-likelihood principle or can be characterized alternatively as the maximum

† E.g. the relative error in the approximation $\sin(\theta/2)\approx\theta/2$ becomes larger than 1% only for angles above 28°.

entropy distribution on the (positive) hypersphere S_+^4 (compare the discussion in Ref. [11]). Additionally, from rotation symmetry and a maximum probability at a chosen orientation $\boldsymbol{x}'$ the (bi-polar) Watson distribution [13]

$$f_W(\boldsymbol{x}) = \frac{1}{N(K)} \exp(K(\boldsymbol{x}\cdot\boldsymbol{x}')^2) \tag{16}$$

$$N(K) = 2\pi^2 \ {}_1F_1(1/2;2;K) \tag{17}$$

follows, where ${}_1F_1$ is the degenerate hypergeometric function and K describes the spread of orientations.

3.3. Disorientation distribution

Because any orientation can be used as the reference orientation, without losing generality the fixed orientation is chosen to be the identity $\boldsymbol{x}' = \pm(1,0,0,0)$ leading to the orientation distribution

$$f_W(\omega,\vartheta,\phi) = \frac{1}{N(K)} \exp(K\cos^2(\omega/2)) = f_W(\omega). \tag{18}$$

The disorientation angle θ between $\mathbf{R}''$ and $\mathbf{R}' = \mathbf{I}$ is then given directly by

$$\cos(\theta/2) = x_0 = \cos(\omega/2) \tag{19}$$

$$\theta = \omega > 0. \tag{20}$$

From the probability of finding a disorientation angle smaller than θ

$$\begin{aligned} \mathrm{P}(X<\theta) &= \iint\int_{\omega\le\theta} f_W(\omega,\vartheta,\phi)\sin^2(\omega/2)\sin(\vartheta)\, d\omega\, d\vartheta\, d\phi \qquad (21) \\ &= 4\pi\int_0^\theta f_W(\omega)\sin^2(\omega/2)\, d\omega \end{aligned}$$

the desired general disorientation distribution on the interval $\theta\in[0,\pi)$

$$\begin{aligned} f_{W,3}(\theta) &= \frac{\mathrm{dP}}{\mathrm{d}\theta} = 4\pi f_W(\theta)\sin^2(\theta/2) \qquad (22) \\ &= \frac{4\pi}{N(K)}\exp(K\cos^2(\theta/2))\sin^2(\theta/2) \end{aligned}$$

is derived.

For small disorientation angles θ the trigonometric functions in equation (22) can be restricted to their leading orders in θ resulting in a simplified distribution

$$f_{W,3}(\theta) \sim \frac{4\pi}{\tilde{N}}\left(\frac{\theta}{2}\right)^2 \exp\left(K\left(1-\frac{\theta^2}{4}\right)\right). \tag{23}$$

With $K = 2/\sigma_\alpha^2$ this is the Maxwell distribution of equation (10) obtained earlier for three independent dislocation sets with perpendicular rotation axes. Note, that the range of the disorientation angle has been changed tacitly to $\theta\in[0,\infty)$ and a different normalization factor $\tilde{N}$ arises.

3.4. Restricted rotation axis

In the previous subsections a uniform distribution of the possible rotation axes $\vec{u}$ on the unit sphere S^3 was assumed. This situation corresponds to the existence of three rotation axes or three equivalent dislocation sets in the boundary, respectively. In a similar way, the combined effect of only two relevant dislocation sets (as two edge dislocation sets in a tilt boundary or one edge dislocation set and screw dislocations in a more general boundary) can be treated. The rotations associated with both dislocation sets act simultaneously, not subsequently. Then all possible rotation axes of the combined rotation are confined in the plane defined by the two individual rotation axes. The resulting rotation axes are all perpendicular to a certain direction and consequently restricted to a unit circle S^2.

The possible rotations form only a subpart of the hemisphere S_+^4 which can be described with e.g. $\vartheta = \pi/2$ ($x_3\equiv 0$) or equivalently by a hemisphere S_+^3 with a reduced dimension. As an analogue to the Watson distribution of equation (18) on S_+^4 the orientation distribution

$$f_W^*(\omega) = \frac{1}{N^*(K)}\exp(K\cos^2(\omega/2)) \tag{24}$$

on S_+^3 is considered. A different normalization factor N^* arises from neglecting x_3 or θ due to the different "volume" element on S_+^3

$$\mathrm{d}V^* = \sin(\omega/2)\,\mathrm{d}\omega\,\mathrm{d}\phi. \tag{25}$$

This leads to the disorientation distribution on the interval $\theta\in[0,\pi)$

$$\begin{aligned} f_{W,2}(\theta) &= 2\pi f_W^*(\theta)\sin(\theta/2) \qquad (26) \\ &= \frac{2\pi}{N^*(K)}\exp(K\cos^2(\theta/2))\sin(\theta/2) \end{aligned}$$

with

$$N^*(K) = 4\pi\int_0^1 \exp(Ku^2)\,\mathrm{d}u. \tag{27}$$

For small angles the disorientation distribution simplifies to the Rayleigh distribution of equation (8) with $K = 2/\sigma_\alpha^2$

$$f_{W,2}(\theta) \sim \frac{2\pi}{\tilde{N}^*}\frac{\theta}{2}\exp\left(K\left(1-\frac{\theta^2}{4}\right)\right). \tag{28}$$

3.5. Relation with distributions for small disorientation angles

Consequently, the distributions derived in Section 2 on the basis of the dislocation content of the boundaries can be seen as asymptotic representations for small angles of the disorientation distributions obtained from orientation distributions proposed on statistical assumptions about orientations (maximum-likelihood principle or maximum entropy [11]).

An application of the more complex distributions for describing experimental data seems not really necessary due to the fact, that there are only small differences between the distributions from equations (22) and (26) and their low disorientation angle pendants of equations (10) and (8). For example, the relative error between the distribution given by equation (22) and a Maxwell distribution is less than 2% in the range $0 \leq \theta \leq 20°$ if both distributions have their maximum at 10°. In case of the distribution given by equation (26) and the Rayleigh distribution the relative error will be even less than 1% for the same conditions.

Of course, for higher disorientation angles the relative errors increase, but for disorientation angles below about 20° the distributions obtained in Section 2 in the limit of small disorientation angles should be sufficient for describing experimental data. Thus, in the following only Rayleigh and Maxwell distributions will be applied.

3.6. Scaling

In contrast to the behaviour of the Maxwell and Rayleigh distribution the distributions of equations (22) and (26) do not show scaling behaviour, even if there is only one parameter K which describes the whole distribution. Due to nonlinearities in θ caused by the trigonometric functions and their periodicity there is no relation like $\langle\theta^m\rangle \propto \bar{\theta}^m$ and scaling by normalization with the average disorientation angle can be validated only in the limit of low disorientation angles. Obviously, the (inherent) periodicity of orientation space prevents true scaling.

4. COMPARISON WITH EXPERIMENTAL DATA

By means of a transmission electron microscope the disorientation angles connected with dislocation boundaries are determined by Liu and Hansen [14, 15] in cold-rolled pure aluminium polycrystals. The inspection of individual boundaries allows the distinction between the two boundary types (IDBs and GNBs) from their morphology. The original data for four different rolling reductions (or plastic strains, respectively) [2, 14] which led to Fig. 1 are evaluated here in a slightly different manner.

Owing to the relatively low disorientation angles (the largest disorientation angle is 15.5°) a comparison of the experimental data with the theoretical distributions is restricted to the findings for small disorientation angles of Section 2. First, the experimental distributions are examined separately for IDBs and GNBs. Later, all boundaries are taken together and the superposition of both distributions is discussed.

4.1. Disorientation angles in IDBs

For each plastic strain the disorientation angles determined for incidental dislocation boundaries are normalized by their average value and the normalized angles $x = \theta/\bar{\theta}$ are gathered into bins of size $\Delta x = \Delta\theta/\bar{\theta}$ (=0.2). The number of occasions N_i in a certain bin i and the total number of measured disorientation angles $N = \sum N_i$ define (an estimation of) the probability

$$\hat{p}_i = \frac{N_i}{N}\frac{1}{\Delta x} \tag{29}$$

to find a normalized disorientation angle in a bin i of width Δx. These relative frequencies (or probability densities) are shown in Fig. 4 for four different strains. All histograms are quite similar and coincide nearly. Based on this observation (or Fig. 1, respectively) scaling of the probability density functions was suggested [2].

The same data are displayed in an alternative way as accumulated frequencies P in Fig. 5. Plotting the probability P of finding a normalized disorientation angle less than x has the opportunity that the disorientation angles need not to be gathered into bins. No information is lost and more details can be revealed compared to the histograms of Fig. 4, even if only

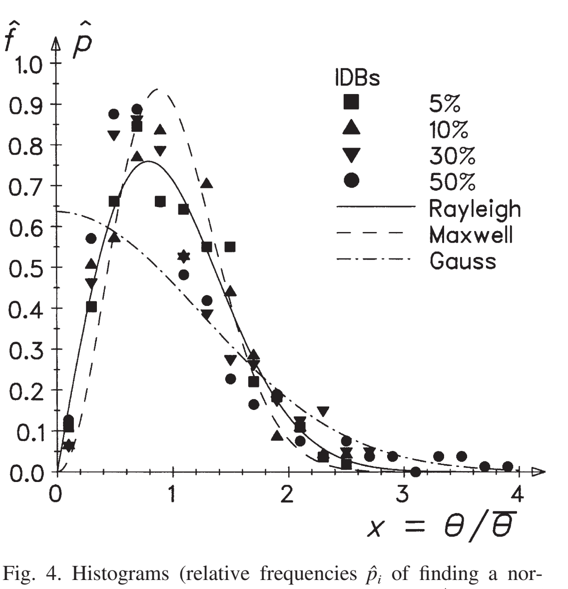

Fig. 4. Histograms (relative frequencies $\hat{p}_i$ of finding a normalized disorientation angle within a bin of width $\Delta x = 0.2$) of the normalized disorientation angles $x = \theta/\bar{\theta}$ of incidental dislocation boundaries in cold-rolled aluminium for different rolling reductions [2, 14]. The lines show the scaled theoretical distributions $\hat{f}(x)$: Rayleigh (equation (9)), Maxwell (equation (12)), and Gauss (equation (A11)).

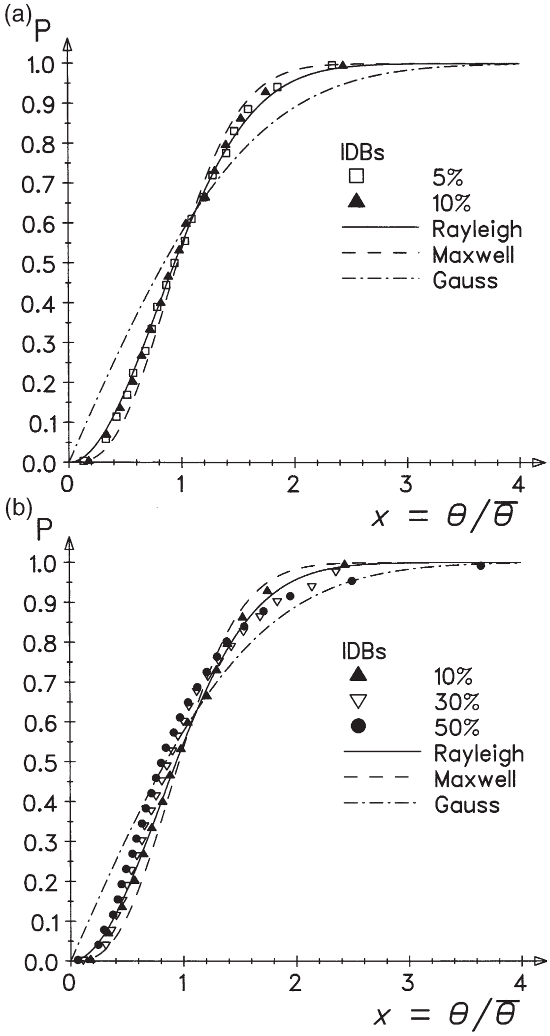

Fig. 5. Accumulated frequencies P of the normalized disorientation angles $x = \theta/\bar{\theta}$ of incidental dislocation boundaries in cold-rolled aluminium for different rolling reductions [2, 14] (only every 15th data point is shown). The lines show the probabilities that a normalized disorientation angle is less than x corresponding to the theoretical distributions: Rayleigh (equation (9)), Maxwell (equation (12)), and Gauss (equation (A11)).

every 15th measurement is shown as a data point as in Fig. 5.

However, in the following always both kinds of representation (as histograms and as accumulated frequencies) are utilized, because they provide complementary information on the shape of the distribution function.

All experimental curves for the different rolling reductions (which are divided up with a view to greater clarity in Fig. 5a and b) are quite similar. No difference at all can be detected between the curves for 5 and 10% in Fig. 5a confirming the scaling hypothesis. From Fig. 5b some deviations of the distributions corresponding to larger strains (30 and 50%) are observed, especially at higher normalized disorientation angles x. These deviations indicate that scaling may not hold exactly as the strain is increased (compare Section 4.5).

The observed deviations can be substantiated further by statistical tests for the similarity of distributions. An estimation for the hypothesis that two empirically obtained data sets belong to the same distribution function can be gained by the Kolmogorow–Smirnow test (e.g. Ref. [16]). This statistical two sample test is based on the accumulated frequencies P of two data samples and the supremum (i.e. maximum) of their difference $|P_1(x)-P_2(x)|$. The probability value (p-value) represents the probability of wrongly rejecting the hypothesis that the two samples belong to the same distribution if it is in fact true. The results of such tests for the data of the scaled disorientation angles $x = \theta/\bar{\theta}$ summarized in Table 2 show that the disorientation data after 5 and 10% are most likely belonging to the same distribution. The same holds to a lesser extent for distributions at subsequent strains, but with increasing difference in rolling reduction any correlation vanishes.

4.2. Comparison with theoretical distributions

The theoretical scaled distributions obtained in Section 2 which contain no fitting parameter are given also in Fig. 4. A comparison with the experimental data (histograms) reveals that a Rayleigh distribution† (equation (9)) describes the experimental data more accurately than the Maxwell distribution (equation (12)) Especially, the width of the Maxwell distribution is too small. This becomes very obvious at angles larger than the mean disorientation angle, for which the Maxwell distribution significantly underestimates their occurrences. However, at very small normalized disorientation angles the histograms in Fig. 4 are not decisive.

That a Rayleigh distribution is more likely than a Maxwell distribution is supported by Fig. 5 where the accumulated frequencies (or the cumulative distribution function)

Table 2. Results (p-values) of Kolmogorov–Smirnov tests on the normalized disorientation angles x for different types of boundaries (IDBs and GNBs): the normalized disorientation angles at two different strains are compared and the probability that the data belong to the same distribution are determined. The result for the normalized disorientation angles $x = \theta/\bar{\theta}_{all}$ from the data taken all boundaries together are also given. Numbers in italic indicate that the hypothesis that the data belong to the same distribution would be rejected for a significance level of 15%

Strains	5%/ 10%	5%/ 30%	5%/ 50%	10%/ 30%	10%/ 50%	30%/ 50%
IDBs	0.99	0.20	*0.01*	0.37	*0.03*	0.42
GNBs	0.33	0.59	0.37	0.75	0.49	0.56
All boundaries	*0.11*	*0.00*	*0.02*	*0.01*	0.59	*0.07*

† Or even a distribution with an inclination angle $\beta \neq 90°$, compare Ref. [4].

$$\mathrm{P} = \int_0^x f(x')\,\mathrm{d}x' \qquad (30)$$

corresponding to the ideal distributions are given also without any fitting and compared with experimental data. Accumulated frequencies and histograms show the same trend: Similarly as seen from the histograms the Rayleigh distribution describes the experimental data best in Fig. 5 for all disorientation angles. Even for small disorientation angles the agreement of the experimentally obtained accumulated frequencies with the Rayleigh distribution is better than with the Maxwell distribution. The data points for 5 and 10% resemble the accumulated frequencies of a Rayleigh distribution remarkably closely and nearly no differences can be detected in Fig. 5a. Even for larger strains (rolling reductions of 30 and 50% in Fig. 5b) where deviations are observed (to be discussed in Section 4.5), the Rayleigh distribution is still a good approximation. Neither a Maxwell distribution (the observed deviations arise in opposite manner compared to a Maxwell distribution) nor a Gaussian distribution (with a vanishing mean value) achieves a good agreement.

Note, that a Gaussian distribution expected for a single dislocation set in the boundary has its maximum at 0°, whereas experimentally determined distributions of the disorientation angles show a maximum at finite angles. The corresponding lack of small disorientations originally led to the proposal of several dislocation sets in a boundary [3].

4.3. Disorientation angles in GNBs

The same evaluation can be performed on the data of geometrically necessary boundaries. Fig. 6a shows the accumulated frequencies P for the normalized disorientation angles x across GNBs for four different plastic strains. Owing to the smaller number of measured boundaries a larger bin size $\Delta x = 0.4$ is chosen in the histograms of Fig. 6b. As noted before, all curves fall closely together confirming the proposed scaling for GNBs [2].

A comparison with theoretical distributions elucidates that the Rayleigh distribution (equation (9)) again gives a better description than a Maxwell distribution of equation (12). But the agreement of the disorientation angle distributions for GNBs (like for the IDBs at higher strains) with a Rayleigh distribution is not as good as in the case of IDBs at small strains. The curves in Fig. 6 give some hints that the maxima of the probability density functions may be shifted to smaller normalized disorientation angles.

Kolmogorow–Smirnow tests (Table 2) give some evidence for the hypothesis that the data sets for the normalized disorientation angles across GNBs at different strains belong to the same distribution function. Table 2 also shows that for the combined data of all boundaries taking together IDBs and GNBs the

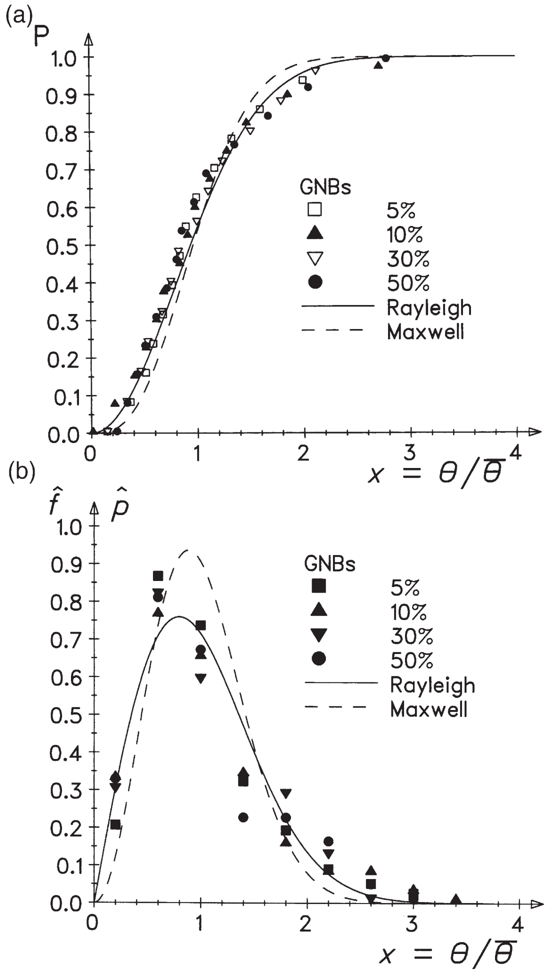

Fig. 6. Normalized disorientation angles $x = \theta/\bar{\theta}$ of geometrically necessary boundaries in cold-rolled aluminium for different rolling reductions [2, 14]: (a) accumulated frequencies P (only every 15th data point is shown); and (b) histograms of relative frequencies $\hat{p}$ for bins of width $\Delta x = 0.4$. The lines show the distributions functions $\hat{f}$ or the corresponding probabilities P that a normalized disorientation angle is less than x for the Rayleigh (equation (9)) and the Maxwell (equation (12)) distribution.

hypothesis of belonging to the same distribution is (almost) always rejected (for a significance level of 15%). This will be discussed in the following subsection.

4.4. Superposition of distributions

As a consequence of the preceding subsections experimental probability densities of the disorientation angles of either IDBs or GNBs may be described in a reasonably good approximation by a Rayleigh distribution. This finding allows the separation of disorientation angles according to the type of the boundaries from data where the disorientation angles of all dislocation boundaries are taken together without distinction between IDBs and GNBs. Accordingly, the combined data are described by a superposition

$$f_{\text{sum}}(\theta) = \xi_{\text{IDB}} f_{\text{R},\bar{\theta}_{\text{IDB}}}(\theta) + \xi_{\text{GNB}} f_{\text{R},\bar{\theta}_{\text{GNB}}}(\theta) = \xi_{\text{IDB}}\bar{\theta}_{\text{IDB}}\hat{f}_{\text{R}}(\theta/\bar{\theta}_{\text{IDB}}) + \xi_{\text{GNB}}\bar{\theta}_{\text{GNB}}\hat{f}_{\text{R}}(\theta/\bar{\theta}_{\text{GNB}}) \quad (31)$$

of two Rayleigh distribution functions corresponding to the two types of boundaries with their relative frequencies (ξ_{IDB} and $\xi_{\text{GNB}} = 1-\xi_{\text{IDB}}$) and average disorientation angles ($\bar{\theta}_{\text{IDB}}$ and $\bar{\theta}_{\text{GNB}}$).

This is illustrated for the experimental data on an aluminium polycrystal cold-rolled to a reduction of 5%, where the disorientation angles of all boundaries (IDBs and GNBs) are taken together as in Fig. 7 and no distinction is made between the two different types of dislocation boundaries. The resulting probability density function in Fig. 7b shows a maximum at the bin centered at 0.5 (from 0.4 to 0.6) with a height of about 0.9. This is obviously in conflict with a Rayleigh distribution (compare Fig. 7b and Table 1), but a fit of a superposition of two Rayleigh distribution functions according to equation (31) (or the corresponding probabilities P, respectively) to the combined data gives the quite close approximation with the parameters $\bar{\theta}_{\text{IDB}} = 0.55°$, $\bar{\theta}_{\text{GNB}} = 1.40°$, and $\xi_{\text{IDB}} = 0.70$ shown in Fig. 7a and b.

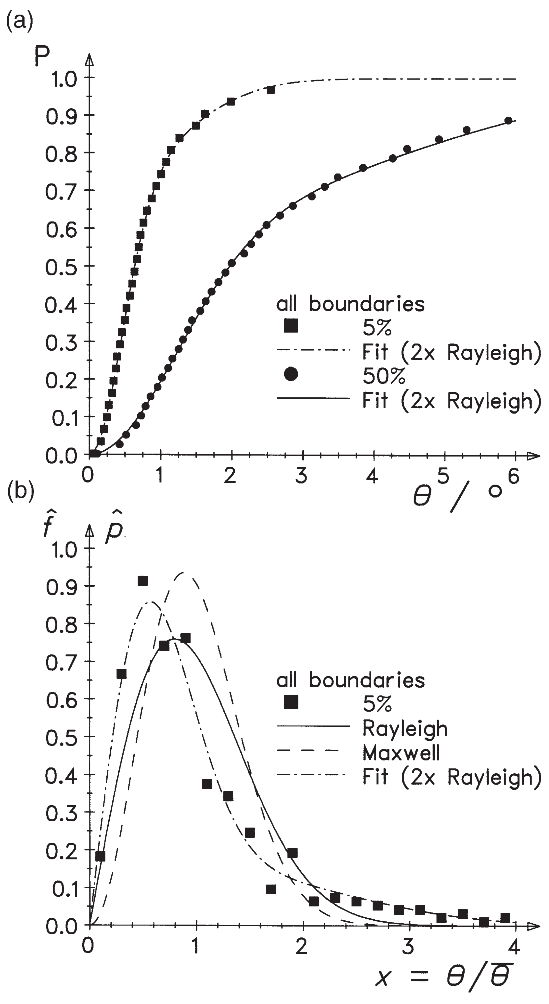

Fig. 7. Disorientation angles from aluminium after 5% cold-rolling for all boundaries (IDBs and GNBs taken together [2, 14]): (a) accumulated frequencies P (only every 15th data point is shown); and (b) histogram (of scaled distributions $\hat{p}$) together with the theoretical distributions $\hat{f}$: Rayleigh (equation (9)) and Maxwell (equation (12)). The dashed dotted line is obtained by fitting according to equation (31) with two Rayleigh distributions of different mean values (in (a) the data for all boundaries after 50% cold-rolling and a similar fit are also included).

On the other hand, the original data set [14] where a distinction between IDBs and GNBs is made has mean values of $\bar{\theta}_{\text{IDB}} = 0.48°$ and $\bar{\theta}_{\text{GNB}} = 1.28°$ and a fraction of 58% of all boundaries is classified as IDBs. Taking into account the uncertainties of the experimental data and of the fitting procedure the results are quite close. Consequently, the two Rayleigh distributions of the fit according to equation (31) in Fig. 7 are closely related to the two different types of boundaries.

A similar fit of a superposition according to equation (31) to the combined data of IDBs and GNBs can be achieved for all rolling reductions (compare the compilation in Table 3 and the graph for 50% in Fig. 7a) confirming the separation into both types of boundaries based on morphology only.

4.5. Distributions at increasing strain

It has been found that a Rayleigh distribution can describe the disorientation angle distributions of IDBs with good accuracy as well as disorientation angle distributions of GNBs. However, some deviations from the ideal Rayleigh distribution† have been observed, for instance, with increasing strain.

In some cases (as for the combined data of IDBs and GNBs in Fig. 7b), experimentally determined

Table 3. Average disorientation angles for IDBs ($\bar{\theta}_{\text{IDB}}$) and GNBs ($\bar{\theta}_{\text{GNB}}$) and fraction ξ_{IBD} of IDBs in cold-rolled aluminium for different rolling reductions: (i) from the individual experimental data sets for each boundary type [2, 14]; and (ii) obtained from the combined data set for all boundaries by fitting of two Rayleigh distributions according to equation (31)

Rolling reduction	(i) Experimental			(ii) Fitting		
	ξ_{IDB}	$\bar{\theta}_{\text{IDB}}$ (°)	$\bar{\theta}_{\text{GNB}}$ (°)	ξ_{IDB}	$\bar{\theta}_{\text{IDB}}$ (°)	$\bar{\theta}_{\text{GNB}}$ (°)
5%	0.58	0.48	1.28	0.70	0.55	1.40
10%	0.53	0.61	1.81	0.61	0.64	1.93
30%	0.68	0.98	4.06	0.64	0.90	3.67
50%	0.67	1.74	5.24	0.59	1.47	4.64

† The Rayleigh distribution is obtained for two equivalent dislocation sets with orthogonal rotation axes. A description with two inclined dislocation sets will not alter the argument, because the distribution function for two dislocation sets given by equations (5) and (7) show only a slight dependence on the inclination angle β. The maximum of the distributions is shifted to lower disorientation angles, but the height of the maximum ($\hat{f}_{\max}\approx 0.76$) remains nearly unaltered [3, 4].

probability densities normalized by their average angles show: (i) a maximum height larger than the maximum height of a scaled Rayleigh distribution $\hat{f}(x_{max})\approx 0.76$; and (ii) simultaneously the maximum occurs at smaller normalized angles than $x_{max}\approx 0.8$ predicted by the scaled Rayleigh distribution. Due to the position of the maximum this can not be explained by the assumption of an equivalent third contribution to the rotation of the boundary and a corresponding scaled Maxwell distribution.

Such deviations may have different cases (to be discussed later) and the experimental data may represent more than a single distribution. In analogy to the combined data for IDBs and GNBs, for these somehow different kind of distributions (which sometimes do not show a proper scaling behaviour, compare Section 5.4) two corresponding Rayleigh distributions for the disorientation angles are considered, but with different average disorientation angles $\bar{\theta}_1$ and $\bar{\theta}_2$. The total disorientation distribution

$$f_{sum}(\theta) = \xi_1 f_{R,\bar{\theta}_1}(\theta) + \xi_2 f_{R,\bar{\theta}_2}(\theta) = \xi_1\bar{\theta}_1\hat{f}_R(\theta/\bar{\theta}_1) + \xi_2\bar{\theta}_2\hat{f}_R(\theta/\bar{\theta}_2) \tag{32}$$

is then a superposition of two Rayleigh distributions with relative frequencies $\xi_i\in[0,1]$ and $\xi_2 = 1-\xi_1$. Due to the overlap of both single distributions usually only one maximum can be seen (as in Fig. 7). An occurrence of a second maximum requires a large ratio between the two mean values $\bar{\theta}_1$ and $\bar{\theta}_2$. Based on the idea of a superposition of two distributions the data for IDBs as well as for GNBs are re-investigated.

4.5.1. IBDs. As shown in Fig. 5b the accumulated frequencies for IDBs after rolling reductions of 30 and 50% deviate slightly from that of a single Rayleigh distribution, but a nice agreement can be obtained by fitting a superposition of two Rayleigh distributions with different mean values as shown in Fig. 8a. Based on this fitting procedure the experimentally determined disorientation angles at larger strains correspond to two different types of IDBs (IDB_1 and IDB_2) with two different mean values, both increasing with strain (compare Fig. 9). At low rolling reductions (5 and 10%) the approximation with a single Rayleigh distribution is quite good and no separation becomes evident. Indeed, fitting of two Rayleigh distributions will result only in a superposition of two distributions with approximately the same mean value.

4.5.2. GNBs. In a similar way, distributions for the disorientation angles of GNBs may be described by a superposition of disorientation angles from GNBs of two different types. Again, a better approximation can be achieved by fitting of a superposition of two Rayleigh distributions than with a single Rayleigh distribution (compare Fig. 8b). As shown in Fig. 9 the different mean disorientation angles of both types (GNB_1 and GNB_2) obtained by fitting increase with strain.

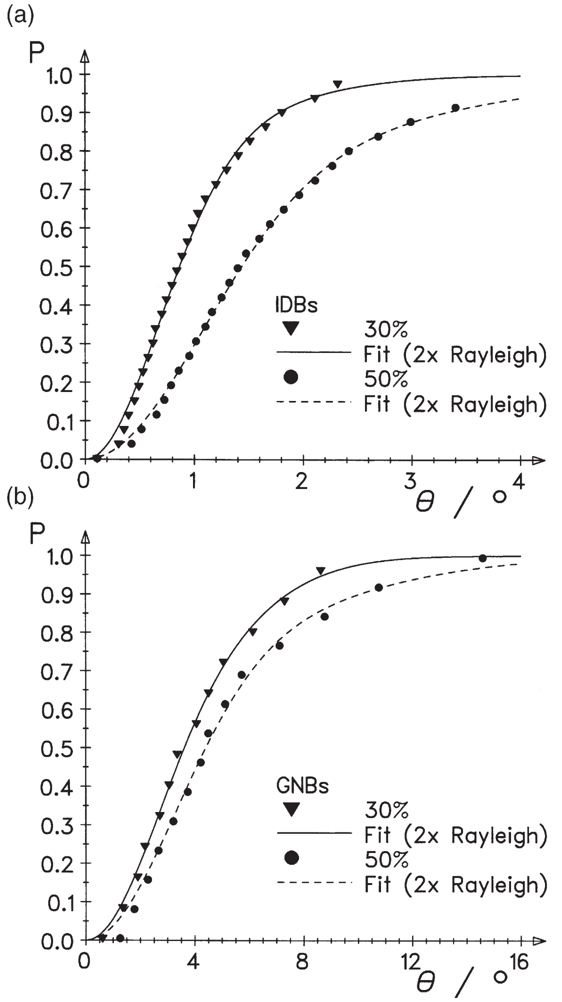

Fig. 8. Accumulated frequencies for the disorientation angles from aluminium after 30 and 50% cold-rolling [2, 14] (only every 15th data point is shown): (a) IDBs; and (b) GNBs. The lines are obtained by fitting with a superposition of two Rayleigh distributions of different mean values according to equation (32).

5. DISCUSSION

5.1. Distribution functions

From geometrical considerations based on different assumptions on the number of dislocation sets and their arrangement, different distribution functions of disorientation angles have been derived, especially the Gauss, the Rayleigh, and the Maxwell distribution. In general, a comparison between these distributions should be based on the scaled versions. The scaled distributions in Fig. 3 or 4 show some significant differences, e.g. the maximum of the scaled Maxwell distribution is higher and occurs at higher normalized disorientation angles than that of the Rayleigh distribution.

More general disorientation distributions (equations (22) and (26)) were obtained from quite general assumptions on the orientations. These disorientation distributions are valid for arbitrarily large

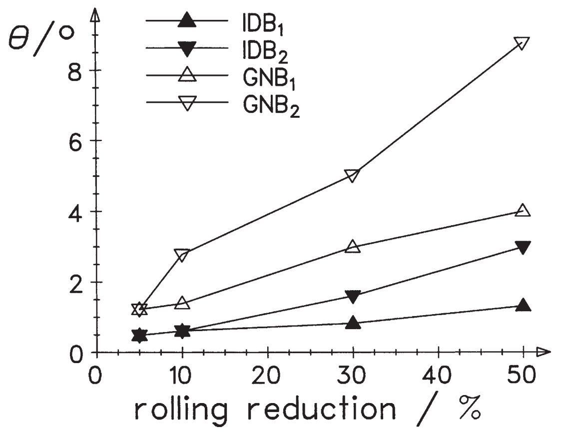

Fig. 9. Mean disorientations angles across different types of IDBs and GNBs in cold-rolled aluminium obtained from fitting with a superposition of two Rayleigh distributions of different mean values according to equation (32). For both types of boundaries no separation was possible for a rolling reduction of 5%, as well as for 10% in the case of IDBs.

disorientation angles and not restricted to smaller angles. Owing to the small differences their low angle approximations, the Rayleigh or Maxwell distribution, are sufficient for an analysis of small disorientation angles (for instance, less than 20°).

5.2. *Agreement with experimental data*

From comparison with experimentally obtained frequency distributions it becomes obvious that a Maxwell distribution shows less agreement than a Rayleigh distribution. A description of the experimental data for IDBs as well as GNBs with Rayleigh distribution indicates, that the rotation associated with a boundary is well described by two dislocation sets. There is no evidence for a significant contribution of a third dislocation set leading to a Maxwell distribution. (If a third dislocation set contributes only marginally, a Rayleigh distribution is still obtained, compare case 2 of Appendix A.)

Ideally, an explanation for the dominance of two dislocation sets in the boundary should be based on the activated slip systems (a task out of the scope of this work). On the other hand, both types of boundaries, IDBs and GNBs, despite their different formation (by statistical trapping or differences in the activation) show the same tendency pointing towards a more basic geometrical reason. It remains unclear, if a contribution of a third set can be excluded for any type of boundaries. The Rayleigh distribution may work in some cases, the Maxwell distribution in others.

5.3. *Superposition of different boundary types*

Experimentally obtained probability density functions with a maximum $\hat{f}_{\max}$ higher than $\hat{f}_{R,\max}\approx 0.76$ at a normalized angle $x_{\max}$ less than $x_{R,\max}\approx 0.8$ (i.e. the corresponding values for a Rayleigh distribution, compare Table 1) are taken as a hint that the distribution does not consist of a single boundary type, but a superposition of two independent distributions from different boundaries.

Superpositions of disorientation angle distributions have been considered in two different cases: (i) All dislocation boundaries taken together without separation into IDBs and GNBs. (ii) Changes in distributions with increasing strain for IDBs and GNBs, respectively. In both cases a good fit of the experimental data is obtained by considering a superposition of two Rayleigh distributions. This is easy to understand for (i) as there is a significant morphological difference between IDBs and GNBs which may indicate a difference in the formation and evolution of these boundaries. Case (ii) is less clear as two IDB distributions (IDB_1 and IDB_2) and two GNB distributions (GNB_1 and GNB_2) are observed. The strain dependence for the average angle of each of these four distributions is shown in Fig. 9. This observation may be understood if the angular evolution of IDBs and GNBs depends on an "unknown" structural parameter, which, for example, could be the crystallographic orientation of the grain in which the boundary is formed. This suggestion is supported by observations on cold-rolled aluminium polycrystals [15], where quite different dislocation structures in grains of different orientation are found. Different relationships between disorientation angle and strain have been observed for IDBs and GNBs, respectively, if the measurements have been classified according to grain orientation. Depending on the grain orientation in some grains GNBs are aligned with slip planes, in other grains not. The average disorientation angles are slightly higher for grains with GNBs not aligned with slip planes than for grains with GNBs on the slip planes for both kinds of boundaries, IDBs and GNBs [15, 17].

These observations motivate the description of, e.g. IDBs, as a mixture of two different types (IDB_1 and IDB_2) at larger strains in Section 4.5. At smaller strains, the orientation effect may be not pronounced enough for causing two significantly different distributions. Up to rolling reductions of 10% only small differences between IDBs in grains of different orientations may occur and the data are well described by a single Rayleigh distribution. Similarly, the existence of two different types of GNBs may be explained by the observed orientation dependence [15, 17]. The formation of GNBs aligned with slip planes (GNB_1) may be quite different from that of GNBs not aligned with slip planes (GNB_2) and the evolution of the disorientation angles across them can be expected to be different for both.

Another explanation of case (ii) may be that the mechanism behind the increase of the disorientation angles changes as the strain is increased. For example, for IDBs their penetrability for mobile dislocations is expected to decrease (respectively, their resistance to dislocation motion is expected to increase) as the disorientation angle increases. For

GNBs, the more pronounced increase of the disorientation angle with strain may lead to changes in the slip pattern in neighbouring crystallites (in principle such an effect corresponds to a change in slip pattern caused by a change in crystal orientation, although on a smaller scale). Alternatively, the increasing deviation from a single Rayleigh distribution with increasing strain may be due to the formation of new boundaries and the resulting distribution may be seen as a superposition of newly formed and matured boundaries.

Considering the different and complex effects it may be an oversimplification to suggest an analysis based on a superposition of only two distributions. However, the calculation shows that a detailed analysis of the disorientation angle distribution may help to elucidate the physical mechanism behind the formation and evolution of dislocation boundaries during plastic deformation.

5.4. Lack of scaling

A superposition of two types of boundaries explains also the lack of scaling for the distributions comprising disorientation angles of all types of boundaries: A different evolution of the two separate average disorientation angles $\bar{\theta}_{\mathrm{IDB}}$ and $\bar{\theta}_{\mathrm{GNB}}$ with strain and an additional change in the relative frequencies of both types of boundaries strongly affect the common mean disorientation angle $\bar{\theta}_{\mathrm{all}} = \xi_{\mathrm{IDB}}\bar{\theta}_{\mathrm{IDB}} + \xi_{\mathrm{GNB}}\bar{\theta}_{\mathrm{GNB}}$. A relation like $\bar{\theta}_{\mathrm{all}} \propto \bar{\theta}_{\mathrm{IDB}} \propto \bar{\theta}_{\mathrm{GNB}}$ would be required for a scaling of the total disorientation distribution given by equation (31), but for IDBs and GNBs such a proportionality does not hold [2, 7, 8]. (An additional complication for the interpretation of combined probability density functions may arise from the ratio of disorientation angles corresponding to both boundary types, compare Table 3.)

6. CONCLUSIONS

The distributions of disorientation angles are discussed in the framework of previously proposed theoretical models [3, 4, 6]. Several constrictions which seem to limit the earlier geometrical approach [3, 4] can be relaxed and even more complicated cases can be treated. For instance, dislocation boundaries with arbitrary tilt or twist character and an arbitrary number of dislocation sets are investigated. The corresponding distribution functions are derived for special cases for small disorientation angles.

It is shown that the distribution functions of disorientation angles obtained from geometrical arguments for small disorientation angles can be derived from quite general assumptions about the distribution of orientations in the limit of low disorientation angles.

The theoretical models are compared with disorientation angles determined after cold-rolling of aluminium polycrystals. It was proved that experimentally determined probability density functions of the disorientation angles are best described by Rayleigh distributions which arise from an equivalent contribution of two dislocation sets in the boundary with perpendicular rotation axes. This type of distribution shows scaling in agreement with previous observations. Deviations from ideal Rayleigh distributions are interpreted as a result of the contributions of different boundaries. For such distributions good descriptions have been obtained by a superposition of two Rayleigh distributions which in general does not show scaling.

In general, it has been found that a detailed analysis of disorientation angle distributions is useful both in a synthesis of experimental data and in an attempt to understand the physical mechanism behind the formation and evolution of dislocation boundaries during plastic deformation.

Acknowledgements—This work was partially performed within the Engineering Science Center for Structural Characterization and Modelling of Materials at Risø. Discussions with Dr N.C. Krieger Lassen on quarternions are gratefully acknowledged. The authors thank Dr Q. Liu for access to the experimental data.

REFERENCES

1. Kuhlmann-Wilsdorf, D. and Hansen, N., *Scripta Metall. Mater.*, 1991, **25**, 1557.
2. Hughes, D. A., Liu, Q., Chrzan, D. C. and Hansen, N., *Acta Mater.*, 1997, **45**, 105.
3. Pantleon, W., *Scripta Mater.*, 1996, **35**, 511.
4. Pantleon, W., *Mater. Sci. Engng. A*, 1997, **234–A236**, 567.
5. Hughes, D. A., Chrzan, D. C., Liu, Q. and Hansen, N., *Phys. Rev.*, 1998, **81**, 4664.
6. Pantleon, W., *Acta Mater.*, 1998, **46**, 451.
7. Pantleon, W., *Mater. Sci. Engng. A*, 2001, in press (special issue of ICSMA-12).
8. Pantleon, W., Dislocation boundaries: formation, orientation and implications, in *Proceedings of the 20th Risø Symposium on Materials Science: Deformation-Induced Microstructures: Analysis and Relation to Properties*, eds J. B. Bilde-Sørensen *et al.*, Risø National Laboratory, Roskilde, Denmark, 1999, p. 123.
9. Read, W. T. and Shockley, W., *Phys. Rev.*, 1950, **78**, 275.
10. Louat, N. P., *Acta Metall.*, 1974, **22**, 721.
11. Schaeben, H., *J. Appl. Cryst.*, 1993, **26**, 112.
12. Bingham, C., *Ann. Stat.*, 1974, **2**, 1201.
13. Watson, G. S., *Biometrika*, 1965, **52**, 193.
14. Liu, Q. and Hansen, N., *Scripta Metall. Mater.*, 1995, **32**, 1289.
15. Liu, Q. and Hansen, N., *Phys. Stat. Sol. (a)*, 1995, **149**, 187.
16. Müller, P. H., *Lexikon der Stochastik*, 5th ed. Akademie Verlag, Berlin, 1991, p. 185.
17. Liu, Q., Juul Jensen, D. and Hansen, N., *Acta Mater.*, 1998, **46**, 5819.
18. Frank, F. C., *Report of a Symposium on Plastic Deformation of Crystalline Solids*. Carnegie Institute of Technology and Office of Naval Research, US Government Printing Office, Washington, 1950, p. 150.

APPENDIX A

General case for small disorientation angles

The most general case of a disorientation with an arbitrary number of dislocation sets in a boundary is considered. It will be shown that for certain simplifications the special results of Section 2 are obtained.

Each of the dislocation sets i contributing to the total orientation difference of the boundary consists of parallel dislocations with Burgers vector $\vec{b}_i$ and a mutual distance ($h = 1/|\vec{N}_i|$) where the vector $\vec{N}_i$ characterizes their density. The disorientation angle θ caused by all dislocations in a boundary free of long-range stresses is given by Frank's formula [18]

$$2\sin(\theta/2)(\vec{p}\times\vec{\rho}) = \sum_{i=1}^{s}(\vec{b}_i\times\vec{N}_i)\cdot\vec{p} \qquad \text{(A1)}$$

with an arbitrary vector $\vec{p}$ in the boundary.

For small disorientation angles the rotation $\theta\vec{\rho} = (\alpha_1,\alpha_2,\alpha_3)$ comprises three independent rotations (α_i) around three orthogonal axes.† These individual rotations are a result of contributions from several dislocation sets. Each dislocation set will lead to a disorientation angle around a certain axis with a normal distributed disorientation angle given by the Read–Shockley formula and a vanishing mean value, e.g. [6, 7]. Dislocation sets corresponding to the same rotation axis can be superimposed directly leading to a Gaussian distribution $f_{G,\sigma}$ for the disorientation angles around this axis. From all possible combinations at most three independent orthogonal rotations can arise with disorientation angles α_1, α_2, and α_3 and their individual standard deviations σ_1, σ_2, and σ_3.

In a first step, the distribution for a combination of rotations around two axes (corresponding to two disorientation angles α_1 and α_2) can be derived along the same lines as before [3]. From

$$P(X<\phi) = \int_{-\phi}^{\phi} d\alpha_1 f_{G,\sigma_1}(\alpha_1)\int_{-\sqrt{\phi^2-\alpha_1^2}}^{\sqrt{\phi^2-\alpha_1^2}} d\alpha_2 f_{G,\sigma_2}(\alpha_2) \qquad \text{(A2)}$$

the distribution of the common disorientation angle ϕ with $\phi^2 = \alpha_1^2 + \alpha_2^2$ is determined

$$f_{\sigma_1,\sigma_2}(\phi) = \frac{dP}{d\phi} = \int_{-\phi}^{\phi} d\alpha_1 f_{G,\sigma_1}(\alpha_1)\frac{2\phi}{\sqrt{\phi^2-\alpha_1^2}} f_{G,\sigma_2}(\sqrt{\phi^2-\alpha_1^2}) \qquad \text{(A3)}$$

† In the limit of infinitesimal rotations no problems arise with the non-commutativity of finite rotations.

$$f_{\sigma_1,\sigma_2}(\phi) = \frac{\phi}{\sigma_1\sigma_2} \exp\left(-\frac{\phi^2}{2}\frac{\sigma_1^2+\sigma_2^2}{2\sigma_1^2\sigma_2^2}\right) I_0\left(\frac{\phi^2}{2}\frac{\sigma_1^2-\sigma_2^2}{2\sigma_1^2\sigma_2^2}\right) \qquad \text{(A4)}$$

which is closely related to the distribution given by equation (5) for two dislocation sets with inclined rotation axes. The same type of distribution for two perpendicular rotations with different standard deviations (equation (A4)) as for two equivalent contributions with equal standard deviations (equation (5)) reveals that both cases even formulated in a very different manner correspond to essentially the same situation. For two equivalent contributions ($\sigma_1 = \sigma_2 = \sigma$) the Rayleigh distribution results

$$f_{\sigma,\sigma}(\phi) = \frac{\phi}{\sigma^2}\exp\left(-\frac{\phi^2}{2\sigma^2}\right) = f_R(\phi). \qquad \text{(A5)}$$

The most general distribution of an angle θ due to three independent contributions around three orthogonal axes ($\theta^2 = \alpha_1^2 + \alpha_2^2 + \alpha_2^3 = \phi^2 + \alpha_3^2$) has to be determined in an analogous manner from

$$P(X<\theta) = \int_{-\theta}^{\theta} d\alpha_3 f_{G,\sigma_3}(\alpha_3)\int_{0}^{\sqrt{\theta^2-\alpha_3^2}} d\phi f_{\sigma_1,\sigma_2}(\phi). \qquad \text{(A6)}$$

The integration cannot be performed in general by elementary methods and has to be done numerically.

But for the special case of two equal contributions (two of the standard deviations are the same $\sigma = \sigma_1 = \sigma_2$ with an arbitrary σ_3) an analytical result

$$f_{\sigma,\sigma,\sigma_3}(\theta) = \frac{\theta}{\sigma\sqrt{\sigma^2-\sigma_3^2}} \exp\left(-\frac{\theta^2}{2\sigma^2}\right)\mathrm{erf}\left(\frac{\theta}{\sqrt{2}}\frac{\sqrt{\sigma^2-\sigma_3^2}}{\sigma\sigma_3}\right) \qquad \text{(A7)}$$

can still be obtained. This leads to three different limiting cases:

1. Three equivalent contributions ($\sigma_3 = \sigma$)

$$f(\theta) = \frac{2\theta^2}{\sqrt{2\pi}\sigma^3}\exp\left(-\frac{\theta^2}{2\sigma^2}\right) = f_M(\theta) \qquad \text{(A8)}$$

   i.e. the Maxwell distribution (10);
2. Only a small contribution of the third rotation ($\sigma_3 \ll \sigma$)

$$f(\theta) = \frac{\theta}{\sigma^2}\exp\left(-\frac{\theta^2}{2\sigma^2}\right) = f_R(\theta) \qquad \text{(A9)}$$

   i.e. the Rayleigh distribution (8);
3. Only a small contribution of two systems and a dominating effect of the third rotation ($\sigma_3 \gg \sigma$)

$$f(\theta) \sim \frac{2}{\sqrt{2\pi}\sigma_3} \exp\left(-\frac{\theta^2}{2\sigma_3^2}\right) \quad \text{(A10)}$$

i.e. a Gaussian distribution leading to a scaled distribution (with $\bar{\theta} = \sigma_3\sqrt{2/\pi}$)

$$\hat{f}(x) = \frac{2}{\pi} \exp\left(-\frac{x^2}{\pi}\right). \quad \text{(A11)}$$

Consequently, the general case simplifies to the special distributions discussed before.